E. Denimal
Department of Mechanical Engineering,
Imperial College London,
London SW7 2AZ, UK
e-mail: e.denimal@imperial.ac.uk

C. Wong
Rolls-Royce plc,
Derby DE2 48J, UK
e-mail: chian.wong@rolls-royce.com

L. Salles
Department of Mechanical Engineering,
Imperial College London,
London SW7 2AZ, UK
e-mail: l.salles@imperial.ac.uk

L. Pesaresi
Department of Mechanical Engineering,
Imperial College London,
London SW7 2AZ, UK
e-mail: l.pesaresi@imperial.ac.uk

On the Efficiency of a Conical Underplatform Damper for Turbines

Underplatform dampers (UPDs) are commonly used in aircraft engines to limit the risk of high-cycle fatigue of turbine blades. The latter is located in a groove between two consecutive blades. The dry friction contact interface between the damper and the blades dissipates energy and so reduces the vibration amplitudes. Two common geometries of dampers are used nowadays, namely wedge and cylindrical dampers, but their efficiency is limited when the blades have an in-phase motion (or a motion close to it), since the damper tends to have a pure rolling motion. The objective of this study is to analyze a new damper geometry, based on a conical shape, which prevents from this pure rolling motion of the damper and ensures a high kinematic slip. The objective of this study is to demonstrate the damping efficiency of this geometry. Hence, in a first part, the kinematic slip is approximated with analytical considerations. Then, a nonlinear dynamic analysis is performed, and the damping efficiency of this new geometry is compared to the wedge and the cylindrical geometries. The results demonstrate that the conical damper has a high damping capacity and is more efficient and more robust than the two others.
[DOI: 10.1115/1.4049665]

Introduction

Industrial requirements in the aerospace industry for gas turbine engines are becoming more stringent in terms of mass and efficiency, so that many components of such structures have reached their structural limits [1]. This is particularly true for turbines blades which are highly loaded, are subjected to high thermal, centrifugal stresses and vibrational stress [2]. The latter can lead to high cycle fatigue and so to the failure of the blades [3]. Since the aero-engines have a large operating speed range and the modal density of bladed disk is high, it is impossible to avoid all critical resonances in the system. Hence, reducing the vibrations levels at these resonances is crucial, and solutions based on friction damping have been the most widely used over the years [4–6].

Dry friction can be introduced in different locations to limit the vibration levels, such as at the shrouds, the roots, and blade tips. However, the most effective solution relies on the use of underplatform dampers (UPD) [6,7]. They consist in a metallic device placed in the groove under the platforms of two adjacent blades. The centrifugal loading keeps them in place during operation. If the blades vibrate, then the relative displacement between the platforms and the damper creates friction at the contact interface and so, energy is dissipated, and the system is damped [8,9].

The identification of the most efficient UPD geometry is still an active research topic. Nevertheless, two main geometries have largely been studied and employed until now. The first shape is based on a wedge geometry [10–15] and the second shape is based on a cylindrical geometry [12,16,17]. Some studies present a combination of the two shapes [18–20] and how to optimize it [21].

The wedge geometry is the shape that is the most widely used over the years. It is easy to manufacture, install and replace, and it seals the platforms. However, with this shape, the prediction of the contact locations and conditions is difficult, which makes the modeling complex and the behavior of the structure difficult to predict [15,22]. Moreover, each damper is loaded in a different way, which complicates even more the global dynamic of the system. The interesting feature of a cylindrical geometry is that the contact pressure is controllable and so the global behavior of the structure is more predictable. However, both shapes have the same limitation. Indeed, when the blades have an in-phase motion, then the damper tends to have a pure rolling motion and no more frictional dissipation occurs. The dissipated energy is null or low, and the damping efficiency is limited.

The objective of this study is to present a new damper geometry based on a conical shape. This geometry makes it impossible for the damper to have a pure rolling motion when the blades have an in-phase motion. In fact, to maintain contact with the two platforms, sliding is required so friction occurs. This friction is directly related to the kinematic motion of the damper created by the in-phase motion of the platform. Hence, the energy dissipated by friction is expected to be high as well as the damping efficiency.

The paper is organized as follows. In a first part, an approximation of the expected kinematic slip of this new damper is determined. It is based on an analytical analysis with a few assumptions. It gives quickly an approximation of the efficiency of the damper with regard to its geometrical characteristics. Then, for more accurate results, a dynamic analysis based on the multiharmonic balance method (MHBM) is done, where the wedge, cylindrical, and conical dampers are compared. The nonlinear receptances as well as the energy dissipated at the contact interface are considered to compare the efficiencies of the different dampers.

New Geometry Presentation and Analytic Performances

Bladed disks are composed of a disk on which blades are fixed, and UPD are located under the platforms of adjacent blades. In this study, the focus is put on a system composed of two blades and one damper. If one considers the first bending mode of the blades, two extreme cases exist: an in-phase motion of the two blades and an out-of-phase motion. It is worth noticing that in reality, the blades have a mix of these two motions, but in the following, only these two "fundamental" conditions will be considered to study the behavior of the damper. Considering these two cases, the kinematic of the platforms can be simplified, respectively, by a pure vertical or a pure horizontal motion of the platforms as illustrated in Fig. 1. For a horizontal motion of the

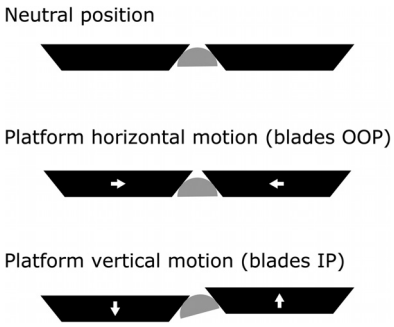

Fig. 1 Illustration of movement of the platforms and the rolling motion

platforms, sliding occurs between the damper and the platforms, so energy is dissipated. However, in the case of a vertical motion, the damper tends to have a pure rolling motion and so the damper efficiency is very limited.

To cope with this issue, a different geometry is presented here. It is based on a conical shape as represented in Fig. 2. The damper is in blue and the planes defined by the platforms are in gray. The main feature of this geometry is that the rolling motion is not possible when a vertical motion of the platforms occurs. Indeed, to keep the contact with the two platforms and to keep its axis parallel to the platforms, the damper cannot have a pure rolling motion and so some sliding must occur. The latter creates friction and so energy is dissipated. This dissipation relies on the pure kinematic motion of the platforms and so a high efficiency of the damper is expected. The study is aimed to demonstrate and illustrate this basic idea. Moreover, this shape presents the advantage to have a robust description of the contact. Indeed, the latter is reduced to a line which is easier to model, locate and gives a more controllable behavior. This section is more specifically dedicated to analytical considerations.

Axial Inclination of the Damper. When the damper is positioned between the two platforms, its axial inclination is fully determined by the cone angle and the angle between the platforms. Moreover, the contact between the damper and each platform corresponds to a line which is also a generator of the cone. An illustration is given in Fig. 2. To determine the cone axial inclination, a few parameters need to be defined:

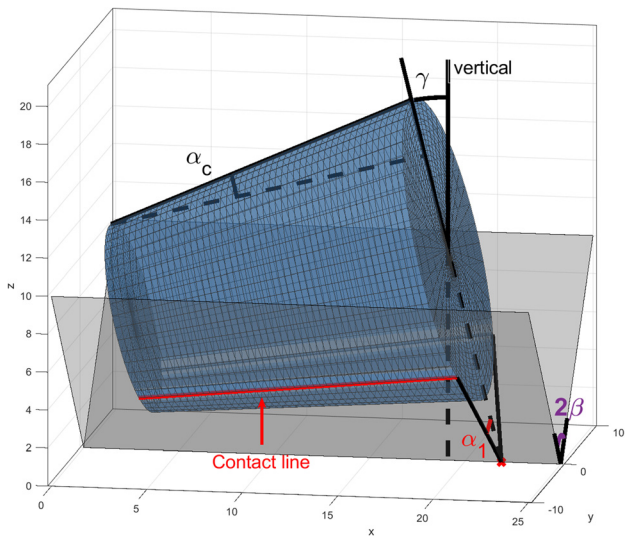

Fig. 2 Illustration of the new damper geometry in contact with the platforms and the angles involved in the geometrical problem

- γ represents the axial inclination of the damper relative to the vertical. It is the angle between the plane formed by a section of the damper and the vertical,
- β is the characteristic angle between the two platforms,
- α_1 corresponds to the projection of the platform angle on the plane formed by the large horizontal section of the damper,
- α_c is the semi-angle of the cone.

The different angles are represented in Fig. 2.

From geometrical considerations, two relations can be obtained to relate the damper inclination γ to the platform angle β and the cone angle α_c

$$\begin{cases} \tan(\alpha_c) = \tan(\gamma) \cdot \sin(\alpha_1) \\ \tan(\alpha_1) = \tan(\beta) \cdot \cos(\gamma) \end{cases} \tag{1}$$

From some manipulations it comes

$$\sin(\gamma)\tan(\beta) = \tan(\alpha_c)\sqrt{(1 + (\cos(\gamma)\tan(\beta))^2)} \tag{2}$$

which gives the following expression of the damper inclination γ in function of the geometrical characteristic of the problem:

$$\gamma(\alpha_c, \beta) = \arccos\left(\frac{\sqrt{(1 - \tan^2(\alpha_c)\cot^2(\beta))}}{\sqrt{\tan^2(\alpha_c) + 1}}\right) \tag{3}$$

From Eq. (3), the effect of the platform angle β and of the cone angle α_c on the damper inclination can be determined. For example, Fig. 3 gives the evolution of the damper inclination depending of the cone angle α_c for different platform angles β. As expected, when the damper is cylindrical, the inclination angle is null, and so the damper is horizontal. On the opposite, when the cone angle becomes equal to the platform angle, then the damper sits in a vertical position at 90 deg with respect to the platforms.

Kinematic Slip. Once the damper inclination is determined, it is possible to get an approximation of the kinematic slip that will occur between the damper and the platforms. The latter is determined when a vertical motion of the platforms occurs, i.e., for the in-phase family of modes of the blades. From this analytical approximation, it is possible to determine the influence of the different parameters on the expected damping efficiency. In order to estimate the kinematic slip, a few assumptions are necessary

- the blades in-phase family of modes is simplified as a pure translational vertical motion between the platforms and the angle between the platforms cannot change,

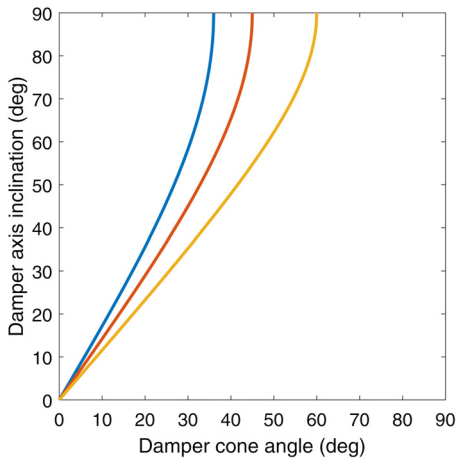

Fig. 3 Damper inclination γ versus the damper cone angle for different platform angles β: $\beta_1 = 36$ deg (blue), $\beta_2 = 45$ deg (orange), and $\beta_3 = 60$ deg (yellow) (see color figure online)

- the damper and the platforms are always in contact,
- the damper and the platforms are perfectly rigid, and no elastic deformation is allowed,
- the middle of the damper is supposed to have a pure rolling motion.

The second and the last points are strong assumptions. The full-contact assumption between the damper and the platforms comes from the idea that from the loading and the conical shape, the damper will always stay stuck to the platforms (no lift-off). The pure rolling motion of the middle section of the damper comes from the idea that the damper tends to have a symmetric motion to have similar displacements at each extremity. It is worth pointing out that these assumptions simplify significantly the problem and are only here to get a quick estimation of the kinematic slip in a preliminary process, rather than giving an accurate estimation of the damping potential for which simulations and tests are required.

Assuming a vertical motion of the platforms v, the vertical component in the plane of the middle section of the damper is $v_t = v \cdot \cos(\gamma)$, illustrated in Fig. 4(*a*). So, if the middle section has a pure rolling motion, then a rotation θ appears with

$$\theta \approx \frac{v_t}{R_m \cos(\alpha_1)} \tag{4}$$

where R_m is the radius of the middle section. The smaller radius is denoted R_1 and the large radius R_2. The angle θ is assuming to be small, which is justified by the fact that the vibration amplitudes are extremely small compared to the geometrical dimensions. At the same time, each extreme section of the damper rotates of the same angle θ. However, the distances traveled by the small and the large sections are different than the distance traveled by the middle section. The difference between the distance traveled by the middle section and the small (respectively large) section of the damper is equal to δ_1 (respectively δ_2)

$$\delta_1 = v_t - \frac{R_1}{R_m} v_t \quad \delta_2 = v_t - \frac{R_2}{R_m} v_t \tag{5}$$

Once the distance δ_1 (respectively δ_2) is traveled by the small (respectively large) section, the latter is not in contact with the other platform. In order to maintain contact with both platforms, it must slip the remaining distance denoted s_1 (respectively s_2). The different configurations of an extreme section of the damper are represented in Fig. 4(*b*). The black configuration corresponds to the initial configuration, the red configuration to the configuration after traveling the distance δ and the blue configuration to the final configuration (i.e., δ and s traveled). Hence, the kinematic slip corresponds to s_1 (respectively s_2) in Fig. 4(*b*) and is equal to

$$s_1 = \frac{\left(1 - \frac{R_1}{R_m}\right)}{\cos(\alpha_1)} v_t \quad s_2 = \frac{\left(1 - \frac{R_2}{R_m}\right)}{\cos(\alpha_1)} v_t \tag{6}$$

A longitudinal kinematic slip s_l also appears and is equal to $s_l = v_s \cos(\alpha_c)$.

As an illustration, the absolute value of the kinematic slip at each position of the damper for different cone angles α_c is given in Fig. 5. The length of the damper is $L = 40$ mm and the platform angle is $\beta = 45$ deg. The kinematic slip is maximum at the extremities of damper and null at the center as expected. Indeed, the main assumption is that the center of the damper has a pure rolling motion, and so does not slip. The evolution is linearly dependent to the distance to the center.

More generally, the maximum expected kinematic slip for different cone angles and for different configuration of the system can be determined. The influence of different parameters is illustrated Fig. 6. In Fig. 6(*a*), the influence of the platform angle β is studied. The evolution of the maximum of the kinematic slip is

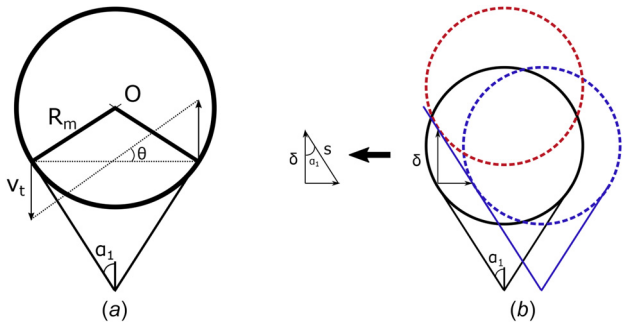

Fig. 4 Kinematic slip determination and position of the damper: (*a*) motion of the middle section of the damper and (*b*) positions of the extreme section of the damper

similar in each case. More precisely, the maximum normalized kinematic slip increases first when the cone angle increases, then it reaches a maximum before decreasing and becoming null when the cone angle is higher than the platform angle (i.e., when the damper has a vertical position). Hence, an increase of the platform angle tends to increase the maximum of the kinematic slip. Moreover, the maximum is reached for different values of the cone angle. Indeed, if $\beta = 36$ deg, the maximum is reached when α_c is around 55% of the platform angle, whereas if $\beta = 60$ deg the maximum is reached around 44% of the platform angle. The influence of the radius of the large section R_1 and of the damper length L is given Figs. 6(*b*) and 6(*c*), respectively. The evolution of the maximum of the kinematic slip is similar than in the case presented previously. However, an increase of the radius R_1 tends to decrease the maximum of expected slip: if $R_1 = 5$ mm then the maximum is around 0.7, whereas if $R_1 = 20$ mm the maximum is around 0.3. Concerning the length of the damper, an increase of the latter tends to increase the maximum of the kinematic slip: if $L = 40$ mm, then the maximum is around 0.4, whereas if $L = 60$ mm then the maximum is around 0.6.

These different analytical considerations provide a coarse estimation of the expected kinematic slip and so of the damper efficiency. Moreover, they allow in a preliminary process to test and compare quickly the impact of some design parameters as the length of the damper, the cone angle, or the radius of the sections.

Comparison With Others Dampers

The analytical results given in the first part can be very useful in a first design process to identify the main characteristics of a damper. However, nonlinear dynamic simulations must be performed to get the real damping performances. The following part is

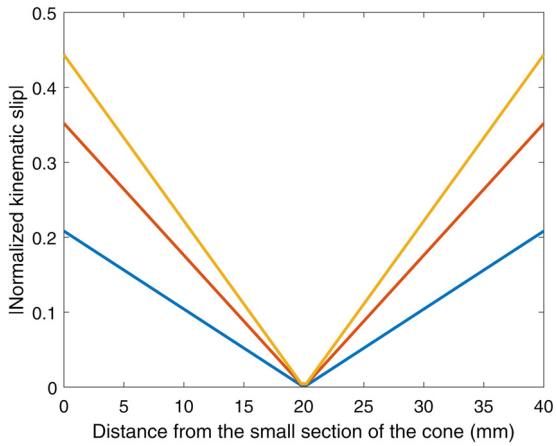

Fig. 5 Evolution of the kinematic slip at each point of the damper for different cone angle: $\alpha_c = 5$ deg (blue), $\alpha_c = 10$ deg (orange), and $\alpha_c = 15$ deg (yellow) (see color figure online)

devoted to the analysis of the performances of the conical damper to validate the analytical approach presented previously. The latter will be compared to a cylindrical and to a wedge damper.

Model Presentation. *Blades model.* The model used is the model of an underplatform test rig, which was used in previous works [15]. It has been designed to experimentally study the effect of UPDs on blade-like structure. The finite element model of the model is represented Fig. 7(*a*) and is composed of two pseudo-beam-like blades that are fixed on a common base which simulates a rigid disk. The dimensions of the model are chosen to mimic the behavior of the dynamic response of a real high pressure turbine blade. The interested reader is invited to refer to Ref. [15] for more information. The mesh is composed of 54,972 quadratic hexahedral elements and a stainless-steel material is used, i.e., the Young modulus is equal to 197 GPa and the density is equal to 7800 kg/m^3. The first two modes of the structure correspond to the first bending mode of the blades, which can be in-phase or out-of-phase. The mode shapes are represented in Figs. 7(*b*) and 7(*c*), respectively.

Damper models. Three damper geometries are considered for this part of the study, they are represented in Fig. 7. The first one is the wedge damper studied in Ref. [15] and represented in Fig. 7(*d*). The second one is a conical damper of cone angle 10 deg represented Fig. 7(*e*). Finally, the third one is a cylindrical damper with a radius equal to the mean radius of the conical damper and is represented in Fig. 7(*f*). The meshes are constructed so that the contact points are matching the blades mesh.

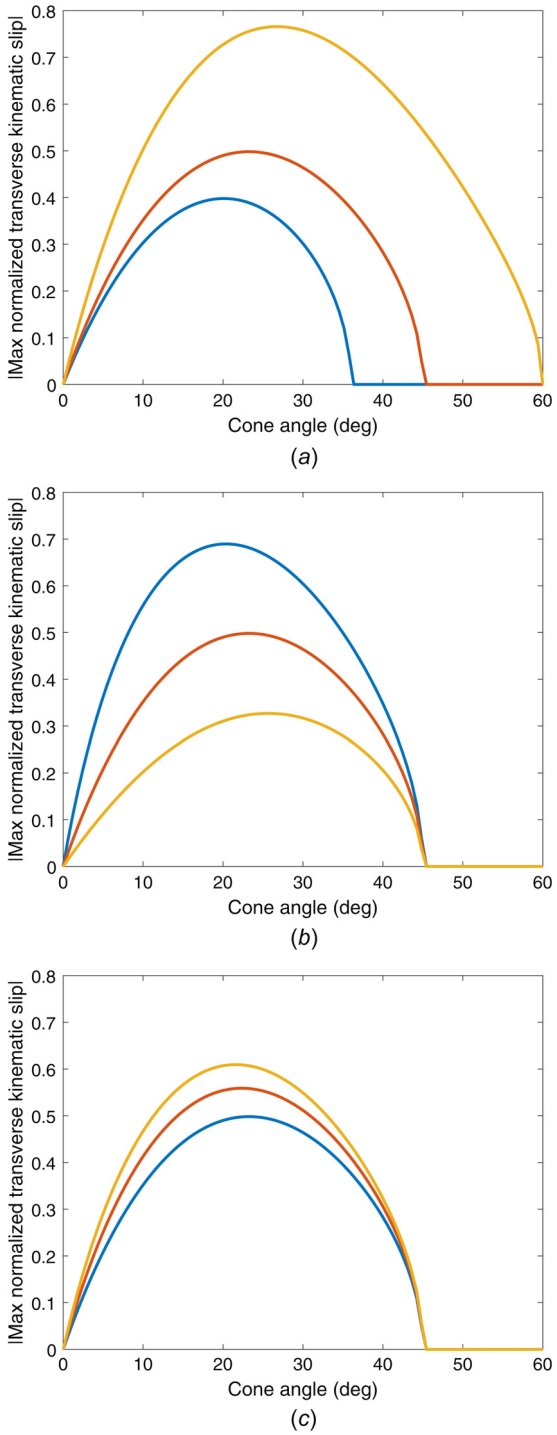

Fig. 6 Influence of different parameters on the maximum kinematic slip with regard to the cone angle α_c: (*a*) maximum kinematic slip versus the cone angle for different platform angles: $\beta_1 = 36$ deg (blue), $\beta_2 = 45$ deg (orange), $\beta_3 = 60$ deg (yellow), (*b*) maximum kinematic slip for different radius R_1 of the cone: $R_1 = 5$ mm (blue), $R_1 = 10$ mm (orange), $R_1 = 20$ mm (yellow), and (*c*) maximum kinematic slip for different length L of the damper: $L = 40$ mm (blue), $L = 50$ mm (orange), and $L = 60$ mm (yellow) (see color figure online)

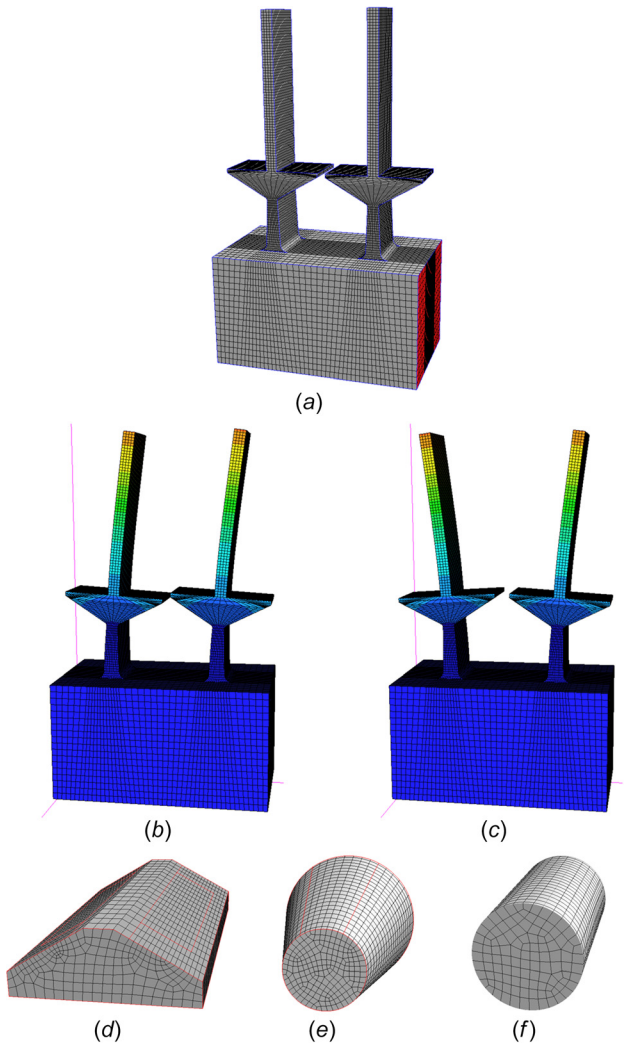

Fig. 7 Finite element model of the blades model (*a*) and the first two modes of the structure ((*b*) and (*c*))—finite element model of the wedge (*d*), conical (*e*), and cylindrical (*f*) dampers: (*a*) mesh of the platforms model, (*b*) in-phase mode $f_{IP} = 269.9$ Hz, (*c*) out-of-phase mode $f_{OOP} = 269.8$ Hz, (*d*) wedge, (*e*) conical, and (*f*) cylindrical

Contact pressure. In all cases, a uniform contact pressure is assumed. For a wedge damper, the contact pressure due the centrifugal loading C_F is modeled by a constant value [11] and the initial pressure σ_0 on each side of the damper is equal to

$$\sigma_0 = \frac{1}{2}\frac{C_F}{A(\cos\alpha + \mu\sin\alpha)} \tag{7}$$

where C_F is the radial centrifugal force, A is the contact area on each side, μ is the friction coefficient, and α is the damper angle. For the cylindrical and the conical damper, it is assumed that the total contact force remains the same. Since the contact between the damper and the platform is a line in these cases, the total contact force is divided by the number of points (the points are regularly positioned).

Contact Formulation. A node-to-node contact formulation is used to solve the problem. Thus, the contact surface of the wedge damper is reduced to 146 points as in Ref. [15], and the contact line for both the cylindrical damper and the conical damper is composed of 23 points (i.e., 46 in total).

The dynamic contact behavior is described at each contact node by the three-dimensional friction contact shown in Fig. 8. This contact model is composed of two decoupled Jenkins elements [4] allowing for two-dimensional in plane displacements, and a third spring is added to allow normal load variations. Hence, each element is characterized by four parameters, namely, the friction coefficient μ, the initial preload N_0, the tangential stiffness k_t, and the normal stiffness k_n. The normal preload and the stiffnesses are normalized by unit of area, so each contact element has its own characteristics. The contact formulation is the same for the different dampers and allows four different states for each point, namely stuck, stick/slip, partial separation and full separation.

Harmonic Balance Method. The numerical strategy used for the prediction of the vibrations levels of the system is based on the MHBM coupled with a model reduction technique included in the in-house code FORSE (FOrced Response SuitE), which is presented in details in Refs. [23–25]. The friction forces from the contact interface bring nonlinearities in the system. The dynamic equation of the system can be written as

$$\mathbf{M}\ddot{\mathbf{X}} + \mathbf{C}\dot{\mathbf{X}} + \mathbf{K}\mathbf{X} + \mathbf{F}_{\mathrm{nl}}(\dot{\mathbf{X}}, \mathbf{X}) = \mathbf{P}(t) \tag{8}$$

where $\mathbf{M}$, $\mathbf{C}$, and $\mathbf{K}$ are the mass, damping, and stiffness matrices, respectively. $\mathbf{X}$ is the vector of displacements and the dot corresponds to the derivative with respect to time. $\mathbf{P}$ is the vector of the external excitation and $\mathbf{F}_{\mathrm{nl}}$ are the nonlinear contact forces that depend of the relative motion of nodes in contact at the interface.

The main idea of the MHBM consists in considering that the response of each DOF is periodic and so can be decomposed on a Fourier series which is truncated at the nth harmonic

$$\mathbf{q}(t) = \mathbf{Q}_0 + \sum_{j=1}^{n} \mathbf{Q}_j^c \cos m_j\omega t + \mathbf{Q}_j^s \sin m_j\omega t \tag{9}$$

where $\mathbf{Q}_0$, $\mathbf{Q}_j^c$, and $\mathbf{Q}_j^s$ are the Fourier coefficients. By injecting Eq. (9) into Eq. (8), and projecting on each harmonic, the system (8) can be approximated by

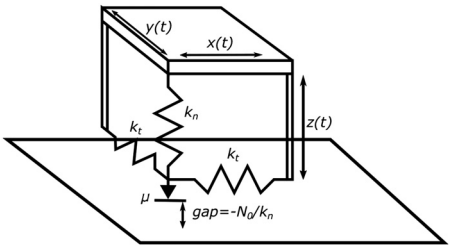

Fig. 8 Contact model

$$\mathbf{Z}(\omega)\mathbf{Q} + \tilde{\mathbf{F}}_{nl}(\mathbf{Q}) - \tilde{\mathbf{P}} = \mathbf{0} \tag{10}$$

where $\mathbf{Q} = \{\mathbf{Q}_0, \mathbf{Q}_1^c, \mathbf{Q}_1^s, \ldots, \mathbf{Q}_n^c, \mathbf{Q}_n^s\}$ is the vector of the Fourier coefficients, $\mathbf{Z}(\omega)$ is the dynamic stiffness matrix of the system, $\tilde{\mathbf{F}}_{\mathrm{nl}}$ and $\tilde{\mathbf{P}}$ are the nonlinear forces and the external efforts in the Fourier basis, respectively. The reduction of the model is based on a frequency response function (FRF) matrix representation of the model. This FRF matrix is determined by calculating its exact value at some frequency points and adding a second term that describes its variation in a range of frequencies [25]. An alternate frequency/time [26,27] algorithm is used for the determination of the nonlinear forces and the problem of Eq. (10) is solved with a Newton–Raphson algorithm. In order to compute a continuous response curve in the frequency domain, continuation is performed with regard to the pulsation ω. Here, a secant predictor together with an arc-length corrector is used. In the following, the harmonics 1, 2, and 3 are used for the simulations. They have been selected based on a convergence study. For the dampers and the blades, 12 modes are used for the simulation.

Comparison of the Performances of the Different Dampers. The nonlinear receptances of the three dampers are computed for different levels of excitation from 0.096 N to 30 N. The receptances are given in Fig. 9 for the out-of-phase family case and in Fig. 10 for the in-phase case.

The nonlinear receptances for the out-of-phase mode are given in Fig. 9 for the three cases. The curves with a solid line correspond to the conical damper receptances, the dashed ones to the cylindrical damper and the dotted ones to the wedge damper. The first observation is that compared to the cylindrical damper, the behavior of the conical damper is almost identical with a small frequency shift of about 0.5 Hz. In all cases, the three dampers have a similar behavior and the damping efficiencies are comparable.

But considering the in-phase case, the behaviors of the three dampers are completely different (see Fig. 10). Indeed, as a first observation, the resonance frequencies are spread from 309 Hz to 423 Hz. As it can be seen in Fig. 10(*b*), all the FRF are superimposed. It demonstrates that the damper has no effect on the dynamic of the blades, in other words the cylindrical damper has a pure rolling motion for this mode and the damping efficiency for this mode is very limited. Hence, the blades have a linear behavior. Considering the wedge damper, it damps the response since the maximum of the receptances decreases when the excitation force increases but it also presents a strong softening behavior and an important frequency shift (around 4 Hz of difference between the peak at $F = 0.096$ N and the peak at $F = 30$ N). Finally, the conical damper presents a behavior similar to the behavior for the

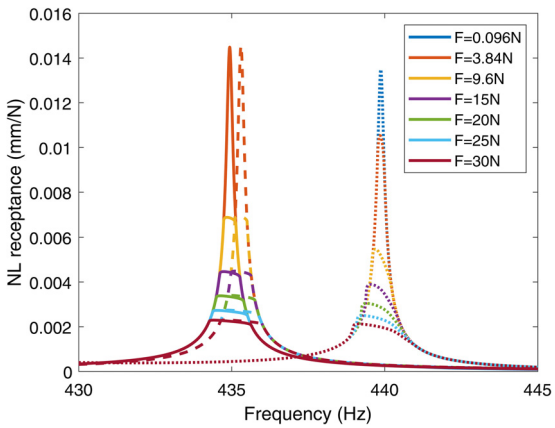

Fig. 9 Nonlinear receptances for the out-of-phase mode: (——) conical damper, (– – –) cylindrical damper, (. . . . .) wedge damper

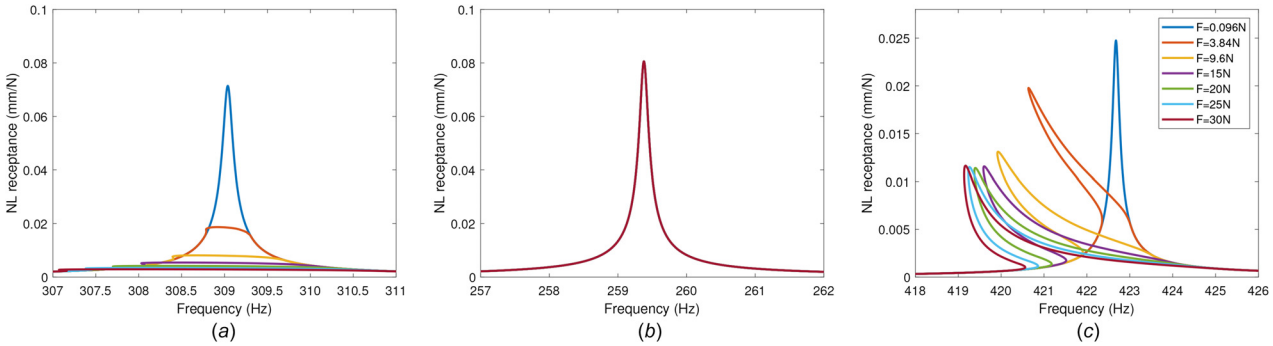

Fig. 10 Nonlinear receptances for the in-phase mode: (left) conical damper—(middle) cylindrical damper—(right) wedge damper: (*a*) conical damper, (*b*) cylindrical damper, and (*c*) wedge damper

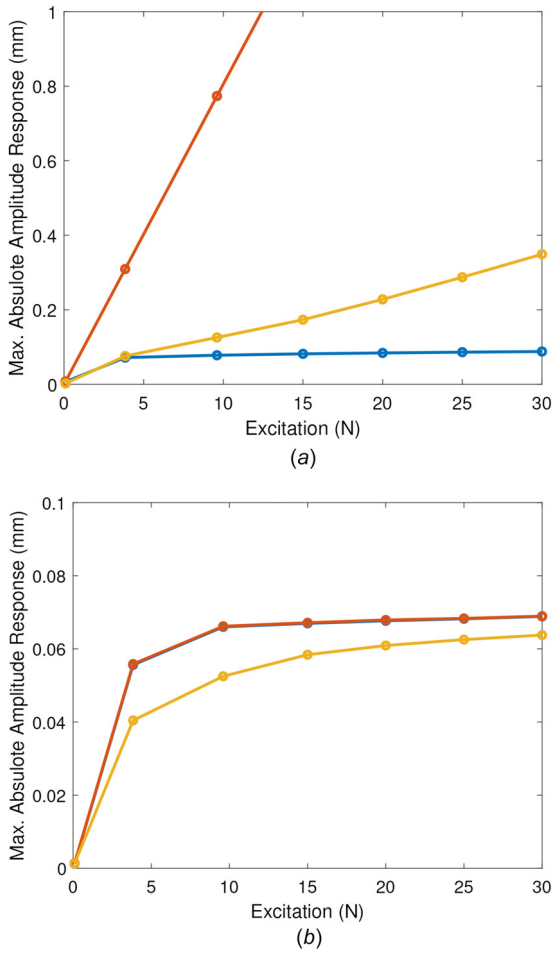

Fig. 11 Maximum of the amplitude response for different level of excitation for the different dampers: (blue) conical damper, (orange) cylindrical, (yellow) wedge damper: (*a*) in-phase mode and (*b*) out-of-phase mode (see color figure online)

out-of-phase mode, i.e., a high damping efficiency without frequency shift [28].

The maximum of the absolute amplitude response is also given for the three dampers in Fig. 11 for the in-phase case (Fig. 11(*a*)) and the out-of-phase case (Fig. 11(*b*)). For the out-of-phase case, the three dampers have a similar behavior. The amplitudes increase when the excitation increases and stabilize between 0.06 mm and 0.07 mm for high excitation levels. For the in-phase case, the three dampers have different behaviors. Indeed, as seen previously, the blades have a linear behavior if the damper is the cylindrical one, so the absolute amplitude increases linearly with the excitation, which gives very high level of amplitude at high level of excitations. For the wedge damper (yellow curve in Fig. 11(*a*)), the maximum of amplitude also increases with the level of excitation but more slowly and reached a maximum of 0.35 mm for $F = 30$ N. But for the conical damper (blue curve), at very low level of excitations, the amplitude response increases but after 5 N, it increases slightly from 7.8×10^{-2} mm at 9.6 N to 8.7×10^{-2} mm at 30 N of excitation amplitude, and almost does not depend of the excitation amplitude. This demonstrates the high damping capacity of the conical damper for the in-phase case. In fact, the damper is even more efficient than the wedge damper since there is a saturation effect.

To investigate more deeply the efficiency of the different dampers, the energy dissipated by friction for the different dampers and the different level of excitation are determined. They are given in Table 1 for the out-of-phase case and in Table 2 for the in-phase case. As expected, the level of energy dissipated by friction for the out-of-phase case is similar for the three dampers. Indeed, the quantity of dissipated energy is almost equal for the three dampers at each level of excitation (see Table 1). However, in the case of the in-phase mode family, the energy dissipated differs a lot from one damper to another. First, the cylindrical damper does not dissipate energy (see the low levels around $\times 10^{-18}$ mJ), which confirms the pure rolling motion of the damper for this case. This analysis is confirmed by the evolution of the contact status of the contact points given in Fig. 12 for the different dampers for excitation levels equal to 9.6 N and 30 N. For the cylindrical and the conical dampers, the points from 1 to 23 correspond to the left contact line, and the points 24 to 46 to the right. They are ordered so that the points 1 and 24 correspond to the large section and the points 23 and 46 to the small section. For the wedge damper, the points 1 to 73 (respectively 74 to 146) correspond to the left (respectively right) contact surface. Red points correspond to

Table 1 Energy dissipated by friction in mJ for the different dampers and the different excitation levels for the out-of-phase mode

Force (N)	0.096	3.84	9.6	15	20	25	30
Wedge	2.3×10^{-22}	1.4×10^{-3}	1.2×10^{-2}	2.6×10^{-2}	3.9×10^{-2}	5.2×10^{-2}	6.6×10^{-2}
Cylindrical	1.3×10^{-21}	1.8×10^{-18}	1.1×10^{-2}	2.4×10^{-2}	3.5×10^{-2}	4.7×10^{-2}	5.8×10^{-2}
Conical	8.1×10^{-22}	1.7×10^{-18}	1.1×10^{-2}	2.3×10^{-2}	3.5×10^{-2}	4.6×10^{-2}	5.8×10^{-2}

Table 2 Energy dissipated by friction in mJ for the different dampers and the different excitation levels for the in-phase mode

Force (N)	0.096	3.84	9.6	15	20	25	30
Wedge	4.7×10^{-21}	3.6×10^{-3}	3.3×10^{-2}	8.1×10^{-2}	1.4×10^{-1}	2.3×10^{-1}	3.3×10^{-1}
Cylindrical	6.2×10^{-23}	1.7×10^{-19}	1.6×10^{-18}	1.0×10^{-18}	4.1×10^{-18}	6.2×10^{-18}	9.5×10^{-18}
Conical	3.9×10^{-20}	1.8×10^{-2}	5.9×10^{-2}	1.0×10^{-1}	1.4×10^{-1}	1.8×10^{-1}	2.2×10^{-1}

cases where stick/slip occurs at the contact and green points where separation occurs. As it can be seen, in the case of the cylindrical damper (top figures), friction occurs only for the out-of-phase case (i.e., at 409 Hz). For the in-phase case, the contact points remain stuck and the damper has a pure rolling motion. Considering the conical damper, stick/slip occurs in both cases, for either the in-phase or the out-of-phase modes. Moreover, for the in-phase case, stick/slip appears at the extremities of the damper

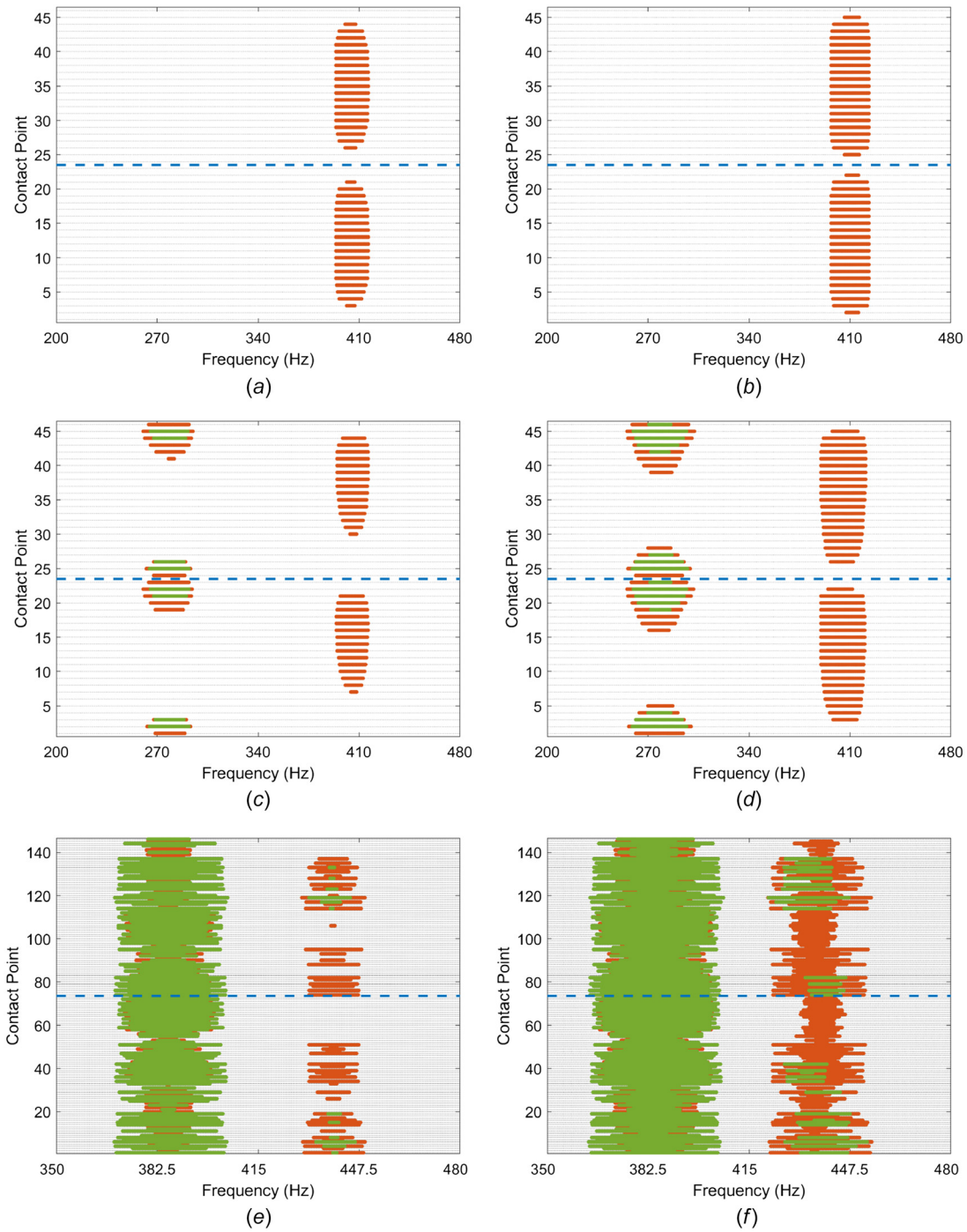

Fig. 12 Evolution of the contacts status for the cylindrical (top), conical (middle), and wedge (bottom) dampers at different frequency levels for an excitation of 9.6 N (left) and 30 N (right): (●) stuck, (●) stick/slip, (●) contact separation, (- - -) separation between contact points on the left side (bottom), and on the right side (top)

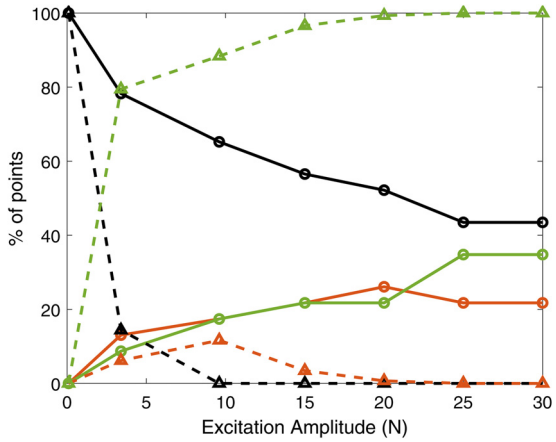

Fig. 13 Evolution of the % of contact condition repartition at the resonance frequency for the conical (——) and the wedge (. . .. . .) for different excitation amplitude, full contact (black), stick/slip (orange), contact separation (green) (see color figure online)

when the center has a pure rolling motion (see the stuck points in the middle of each contact line). This confirms the assumption done in the analytical part. Moreover, no full contact separation is observed for the different amplitudes of excitation, justifying the full-contact assumption done in the analytical part. Since stick/slip occurs for the in-phase case, some energy is dissipated by friction and so the damper has, as expected, a damping effect on the system. Considering the wedge damper, the dynamic of the contact is much more complex for the in-phase case since almost all points experience contact separation (see Figs. 12(*e*) and 12(*f*)). This illustrates the rolling motion of the damper and explains the strong softening behavior observed in Fig. 10(*c*).

For more insight, the evolution of the repartition of the contact condition at the first resonance frequency for both the wedge and the conical dampers for different excitation amplitudes is given Fig. 13. As it can be seen, for the conical damper (solid lines) the number of contact points in a stick/slip or partial contact state increases when the excitation amplitude increases. This evolution may explain why the maximum of the amplitude response remains almost constant in Fig. 11(*a*) for the conical damper. Considering the wedge damper, when the excitation amplitude increases, all the points tend to experience contact separation. The energy dissipated by friction by the wedge damper in the in-phase case is of the same order of magnitude than the energy dissipated by the conical damper. Hence, the conical and the wedge dampers have similar performances in terms of energy dissipation. However, the results obtained here for the wedge damper are based on the strong assumption that the contact surface is in perfect contact. In reality, the location and the surface area of the contact are unknown, and it results in a drop of the resonance frequency for this mode. Hence, the modeling of this damper is limited, and the resonance frequency cannot be estimated. On the opposite, the contact condition between the conical damper and the platforms is much more robust since it corresponds to a contact line that can be easily identified. It results in a strong ability to model and capture the behavior of the structure. Moreover, the coupling between the platforms can be controlled, and so the frequency shift caused by the damper. For these different reasons, the conical damper appears more efficient and reliable than the wedge damper.

Conclusion

In this study, a new damper geometry has been evaluated. Based on a conical geometry, the problem of pure rolling motion when the blades have an in-phase motion cannot occur. Indeed, to maintain contact with the two platforms, slipping motion must takes place, and so friction appears. This friction is due to the pure kinematic motion of the platforms, and so the conical damper has a very high damping potential.

First, from geometrical considerations and some assumptions, an analytical formulation of the expected kinematic slip is determined. It allows a fast estimation of the performances of a damper for different geometric properties in a preliminary design process. Then, the real damping efficiency of the damper is determined by using a nonlinear dynamic analysis based on the HBM. The nonlinear receptances of the conical damper for different excitation levels are compared to the receptances of a cylindrical and a wedge damper. The damping properties of the different dampers are similar in the case of an out-of-phase motion of the blades. But in the case of an in-phase motion of the blades, the behaviors of the three dampers tend to be very different. The cylindrical damper has a pure linear behavior and has almost no damping properties. The wedge damper has a strong softening behavior, and so a non-negligible frequency shift. On the opposite, the conical damper has a high level of damping as it was expected from the analytical results. The energy dissipated by friction for the different dampers are almost compared and confirmed the pure rolling motion of the cylindrical damper in in-phase case. The energies dissipated by the wedge and the conical damper are of the same order of magnitude.

As a conclusion, the conical damper has a high damping potential for both in-phase and out-of-phase motion. The contact conditions are more robust than for the wedge damper since the contact corresponds to a contact line that can be easily located. Moreover, by increasing the cone angle, the coupling effect between the two platforms is increased; therefore, the frequency shift caused by the damper can be controlled by a simple controllable parameter. Furthermore, from simple design parameters (as the cone angle), a very fine tradeoff between the damping efficiency and the wear rate can be achieved.

Acknowledgment

The third and fourth authors are grateful to Innovate UK (Grant No. MEDY.P50254) and Rolls-Royce plc (Grant No. MEDY.P42978) for providing the financial support for this work and for giving permission to publish it. This work was part of a collaborative R&T project SILOET II P19.6 which is cofunded by Innovate UK and Rolls-Royce plc. The first and third authors thank Rolls-Royce plc and the EPSRC for the support under the Prosperity Partnership Grant "Cornerstone: Mechanical Engineering Science to Enable Aero Propulsion Futures," Grant Ref: EP/R004951/1.

Funding Data

- Engineering and Physical Sciences Research Council (Grant Ref. EP/R004951/1; Funder ID: 10.13039/501100000266).
- Innovate UK (Grant No. MEDY.P50254; Funder ID: 10.13039/501100006041).
- Rolls-Royce (Grant No. MEDY.P42978; Funder ID: 10.13039/501100000767).

References

[1] Krack, M., Salles, L., and Thouverez, F., 2017, "Vibration Prediction of Bladed Disks Coupled by Friction Joints," Arch. Comput. Methods Eng., **24**(3), pp. 589–636.

[2] Petrov, E., and Ewins, D., 2004, "State-of-the-Art Dynamic Analysis for Non-Linear Gas Turbine Structures," Proc. Inst. Mech. Eng., Part G, **218**(3), pp. 199–211.

[3] Cowles, B., 1996, "High Cycle Fatigue in Aircraft Gas Turbines—An Industry Perspective," Int. J. Fract., **80**(2–3), pp. 147–163.

[4] Gaul, L., and Nitsche, R., 2001, "The Role of Friction in Mechanical Joints," Appl. Mech. Rev., **54**(2), pp. 93–106.

[5] Feeny, B., Guran, A., Hinrichs, N., and Popp, K., 1998, "A Historical Review on Dry Friction and Stick-Slip Phenomena," Appl. Mech. Rev., **51**(5), pp. 321–341.

[6] Griffin, J., 1990, "A Review of Friction Damping of Turbine Blade Vibration," Int. J. Turbo Jet Engines, **7**(3–4), pp. 297–308.

[7] Szwedowicz, J., Gibert, C., Sommer, T., and Kellerer, R., 2008, "Numerical and Experimental Damping Assessment of a Thin-Walled Friction Damper in the Rotating Setup With High Pressure Turbine Blades," ASME J. Eng. Gas Turbines Power, **130**(1), p. 012502.

[8] Sanliturk, K., Ewins, D., and Stanbridge, A., 2001, "Underplatform Dampers for Turbine Blades: Theoretical Modeling, Analysis, and Comparison With Experimental Data," ASME J. Eng. Gas Turbines Power, **123**(4), pp. 919–929.

[9] Sanliturk, K., Ewins, D., Elliott, R., and Green, J., 2001, "Friction Damper Optimization: Simulation of Rainbow Tests," ASME J. Eng. Gas Turbines Power, **123**(4), pp. 930–939.

[10] Panning, L., Popp, K., Sextro, W., Kayser, A., and Wolter, I., 2004, "Asymmetrical Underplatform Dampers in Gas Turbine Bladings: Theory and Application," ASME Paper No. GT2004-53316.

[11] Petrov, E., and Ewins, D., 2007, "Advanced Modeling of Underplatform Friction Dampers for Analysis of Bladed Disk Vibration," ASME J. Turbomach., **129**(1), pp. 143–150.

[12] Panning, L., Sextro, W., and Popp, K., 2000, "Optimization of Interblade Friction Damper Design," ASME Paper No. 2000-GT-0541.

[13] Jareland, M., 2001, "A Parametric Study of a Cottage-Roof Damper and Comparison With Experimental Results," ASME Paper No. 2001-GT-0275.

[14] Firrone, C., Zucca, S., and Gola, M., 2009, "Effect of Static/Dynamic Coupling on the Forced Response of Turbine Bladed Disks With Underplatform Dampers," ASME Paper No. GT2009-59905.

[15] Pesaresi, L., Salles, L., Jones, A., Green, J., and Schwingshackl, C., 2017, "Modelling the Nonlinear Behaviour of an Underplatform Damper Test Rig for Turbine Applications," Mech. Syst. Signal Process., **85**, pp. 662–679.

[16] Jareland, M., 2001, "Experimental Investigation of a Platform Damper With Curved Contact Areas," ASME Paper No. DETC2001/VIB-21391.

[17] Csaba, G., 1999, "Modelling of a Microslip Friction Damper Subjected to Translation and Rotation," ASME Paper No. 99-GT-149.

[18] Bessone, A., Toso, F., and Berruti, T., 2015, "Investigation on the Dynamic Response of Blades With Asymmetric Under Platform Dampers," ASME Paper No. GT2015-42597.

[19] Gola, M., and Gastaldi, C., 2014, "Understanding Complexities in Underplatform Damper Mechanics," ASME Paper No. GT2014-25240.

[20] Zucca, S., Botto, D., and Gola, M., 2008, "Range of Variability in the Dynamics of Semi-Cylindrical Friction Dampers for Turbine Blades," ASME Paper No. GT2008-51058.

[21] Gastaldi, C., and Gola, M., 2017, "Pre-Optimization of Asymmetrical Underplatform Dampers," ASME J. Eng. Gas Turbines Power, **139**(1), p. 012504.

[22] Pesaresi, L., Armand, J., Schwingshackl, C., Salles, L., and Wong, C., 2018, "An Advanced Underplatform Damper Modelling Approach Based on a Microslip Contact Model," J. Sound Vib., **436**, pp. 327–340.

[23] Petrov, E., and Ewins, D., 2003, "Analytical Formulation of Friction Interface Elements for Analysis of Nonlinear Multi-Harmonic Vibrations of Bladed Disks," ASME J. Turbomach., **125**(2), pp. 364–371.

[24] Petrov, E., 2008, "Explicit Finite Element Models of Friction Dampers in Forced Response Analysis of Bladed Disks," ASME J. Eng. Gas Turbines Power, **130**(2), p. 022502.

[25] Petrov, E., 2011, "A High-Accuracy Model Reduction for Analysis of Nonlinear Vibrations in Structures With Contact Interfaces," ASME J. Eng. Gas Turbines Power, **133**(10), p. 102503.

[26] Cameron, R., and Martin, W., 1947, "The Orthogonal Development of Non-Linear Functionals in Series of Fourier-Hermite Functionals," Ann. Math., **48**(2), pp. 385–392.

[27] Salles, L., Blanc, L., Thouverez, F., Gouskov, A., and Jean, P., 2009, "Dynamic Analysis of a Bladed Disk With Friction and Fretting-Wear in Blade Attachments," ASME Paper No. GT2009-60151.

[28] Ning, X., and Lovell, M., 2002, "On the Sliding Friction Characteristics of Unidirectional Continuous FRP Deposits," ASME J. Tribol., **124**(1), pp. 5–13.